NBO, HOMO, LUMO analysis and vibrational spectra (FTIR and FT Raman) of 1-Amino 4-methylpiperazine using ab initio HF and DFT methods

ARTICLE *in* SPECTROCHIMICA ACTA PART A MOLECULAR AND BIOMOLECULAR SPECTROSCOPY · JULY 2014

Impact Factor: 2.35 · DOI: 10.1016/j.saa.2014.06.157 · Source: PubMed

2 AUTHORS:

Govindaraj Mahalakshmi

Karpagam University

8 PUBLICATIONS **34** CITATIONS

SEE PROFILE

Dr Vadivelu Balachandran

A.A.Government Arts College Musiri

155 PUBLICATIONS **672** CITATIONS

SEE PROFILE

Spectrochimica Acta Part A: Molecular and Biomolecular Spectroscopy 131 (2014) 587–598

Contents lists available at ScienceDirect

Spectrochimica Acta Part A: Molecular and Biomolecular Spectroscopy

journal homepage: www.elsevier.com/locate/saa

Molecular structure, vibrational spectra (FTIR and FT Raman) and natural bond orbital analysis of 4-Aminomethylpiperidine: DFT study

G. Mahalakshmi [a,b], V. Balachandran [c,*]

[a] Department of Physics, Karpagam University, Coimbatore 641 021, India
[b] Department of Physics, Government Arts College (Autonomous), Karur 639 005, India
[c] Research Department of Physics, Arignar Anna Government Arts College, Musiri, Tiruchirappalli 621 211, India

HIGHLIGHTS

- Molecular conformers of 4-Aminomethylpiperidine were investigated.
- Spectroscopic properties of 4-Aminomethylpiperidine were examined.
- Torsional potential energy surface (PES) scan studies were recorded.
- The complete assignments are performed on the basis of potential energy distribution (PED).

GRAPHICAL ABSTRACT

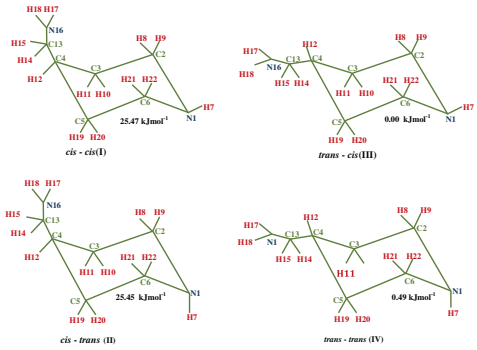

ARTICLE INFO

Article history:
Received 12 January 2014
Received in revised form 19 April 2014
Accepted 23 April 2014
Available online 6 May 2014

Keywords:
FT-IR
FT-Raman
Intramolecular hydrogen bond
NBO
HOMO–LUMO
4-Aminomethylpiperidine (4AMP)

ABSTRACT

The FT-IR and FT-Raman spectra of 4-Aminomethylpiperidine have been recorded using Perkin Elmer Spectrophotometer and Nexus 670 spectrophotometer. The equilibrium geometrical parameters, various bonding features, the vibrational wavenumbers, the infrared intensities and the Raman scattering activities were calculated using Hartree–Fock and density functional method (B3LYP) with 6-311+G(d,p) basis set. Detailed interpretations of the vibrational spectra have been carried out with the aid of the normal coordinate analysis. The spectroscopic and natural bonds orbital (NBO) analysis confirms the occurrence of intra molecular hydrogen bonds, electron delocalization and steric effects. The changes in electron density in the global minimum and in the energy of hyperconjugative interactions of 4-Aminomethylpiperidine (4AMP) were calculated. The theoretical UV–Visible spectrum of the compound was computed in the region 200–400 nm by time-dependent TD-DFT approach. The calculated HOMO and LUMO energies show that charge transfer occur within the molecule. The dipole moment (μ) and polarizability (α), anisotropy polarizability ($\Delta\alpha$) and hyperpolarizability (β) of the molecule have been reported.

Introduction

Piperidine is a widely used building block and chemical reagent in the synthesis of organic compounds, including pharmaceuticals. The piperidine structural motif is present in numerous natural alkaloids. Piperidine is obtained from black pepper, from *Psilocaulonabsimile* N.E.Br (Aizoaceae), and in *Petrosimoniamonandra* [1–3]. It is also found in the fire ant's toxin–solenopsin, the nicotine analog anabasine of the Tree Tobacco (*Nicotianaglauca*), lobe line of the Indian tobacco, and the toxic alkaloid coniine from poison hemlock, which was used to put Socrates to death [4,5]. Piperidine

* Corresponding author. Tel.: +91 431 2591338; fax: +91 4326 262630.
E-mail address: brsbala66@gmail.com (V. Balachandran).

http://dx.doi.org/10.1016/j.saa.2014.04.154
1386-1425/

is a widely used secondary amine. It is widely used to convert ketones to enamines [6]. Enamines derived from piperidine can be used in the Stork enamine alkylation reaction [7]. Piperidine can be converted to the chloramines $C_5H_{10}NCl$ with calcium hypochlorite. The resulting chloramine undergoes dehydrohalogenation to afford the cyclic imine [8]. Piperidine and its derivatives are ubiquitous building blocks in the synthesis of pharmaceuticals and fine chemicals. The piperidine structure is found in the pharmaceuticals. For example SSRI (Selective Serotonin Reuptake Inhibitors), SERM (Selective Estrogen Receptor Modulators), Vasodilators, Neuroleptics (Antipsychotics), Opioids and Psychochemical compounds.

Piperidine is also commonly used in chemical degradation reactions, such as the sequencing of DNA in the cleavage of particular modified nucleotides. Piperidine is also commonly used as a base for the deprotection of Fmoc (Fluorenylmethyloxycarbonyl)-amino acids used in solid-phase peptide synthesis. Piperidine is precursor under the United Nations Convention Against Illicit Traffic in Narcotic Drugs and Psychotropic Substances due to its use (peaking in the 1970s) in the clandestine manufacture of Phenylcyclohexylpiperidine (PCP) (also known as angel dust, sherms, wet, etc.). Pyridine and its derivatives are very important in industrial field as well as in biochemistry. Pyridine can also be reduced to piperidine by sodium in ethanol [9].

The main objective of the present study is to investigate in detail the conformational stability and vibrational spectra of 4AMP using density functional theory (DFT) method, which can presumably help in understanding its dynamical behavior. The characterization of the normal modes using potential energy distribution was done with the MOLVIB-7.0 program. In the present work, we have attempted to study the bonding nature of 4AMP using B3LYP level of theory throughout with the 6-311+G(d,p) basis set [10] implemented in the Gaussian 09 program suite [11]. Geometries obtained from DFT calculation were then used to perform NBO analysis.

Experimental

The title compound was obtained from Sigma Aldrich, U.S.A and used as such to record FT-IR and FT-Raman spectra. The FT-Raman spectrum of 4AMP was recorded in the region 4000–400 cm^{-1} using 1064 nm line of Nd:YAG laser as excitation wave length on thermo electron corporation model Nexus 670 spectrophotometer equipped with FT-Raman module accessory. The FT-IR spectrum of the title compound was recorded in the region 4000–0 cm^{-1} on Perkin Elmer Spectrophotometer and KBr pellet technique.

Computational methods

The geometrical parameters of 4AMP have been optimized using the HF and B3LYP level of theory implementing the 6-311+G(d,p) basis set, using the 2009 version of the Gaussian suite program [11]. The characteristic vibrational frequencies for 4AMP were calculated using the same level of theory. The vibrational frequencies calculated in HF method with 6-311+G(d,p) level of basis set were scaled by 0.9079 for wavenumbers above 1500 cm^{-1} and 0.8649 for below 1500 cm^{-1}. The scaled values used in B3LYP/6-311+G(d,p) were 0.9512 for wavenumbers less than 1000 cm^{-1} and 0.9149 for higher wavenumbers. After scaling factor, the deviations from the experiment values are reliable. Transformation of the force field and subsequent normal coordinate analysis including the least square refinement of the scale factors, calculation of the potential energy distribution [PED] and the prediction of FT-IR and FT-Raman intensities were done on a PC with the MOLVIB Program (version 7.0G77) written by Sundius [12]. The Raman activities (s_i) calculated by Gaussian 09 program has been converted to relative Raman intensities (I_i).

The natural bonding orbitals (NBO) calculations [13] were performed at the DFT/B3LYP level in order to investigate the electronic structures of the optimized geometry. The hyperconjugative interaction energy was deduced from the second-order perturbation approach [14]

$$E^{(2)} = \Delta E_{ij} = q_i \frac{F_{(i,j)^2}}{\varepsilon_j - \varepsilon_i}$$

where q_i is the ith donor orbital occupancy, ε_j, ε_i the diagonal elements (orbital energies) and (j,i) the off diagonal NBO Fock Matrix element. The first and second hyperpolarizability of 4AMP have been calculated using the same method. The HOMO–LUMO analysis has been carried out to explain the charge transfer within the molecule. The electron donor and acceptor atoms of the compound were also identified with the aid of molecular electrostatic potential (MEP) surface.

Results and discussion

In order to find out the most optimized geometry, the energy calculations were carried out for various possible conformers. The possible four conformers *cis-cis*(I), *cis–trans*(II), *trans–cis*(III), *trans–trans*(IV) and their corresponding relative energies of 4AMP are shown in Fig. 1. It is clear from Fig. 1 that the conformer *trans–cis*(III) has produced the global energy minimum. The most optimized geometrical parameters were calculated for 4AMP of *trans–cis*(III) conformer by HF and B3LYP methods with 6-311+G(d,p) basis set. The bond lengths and bond angles are determined from geometrical parameters obtained from HF and DFT method. The geometrical parameters obtained from DFT method are seen in good agreement with experimental values of X-ray data [15] and the deviations are due to the presence of amino and methyl groups. Therefore, the experimental X-ray data are compared only with the DFT method and they are summarized in Supplementary data (S1). In the literature, we have found neither experimental data nor calculation for molecular geometric structure of 4AMP. It is known that the six-member cyclic molecule piperidine and 4-methyl piperidine ring exist in chair forms to can in principle as conformers with N–H being equatorial (E) and axial (A) [16–19]. Other conformations that differ from the chair (boat, envelope or twist boat) were not considered because of their high energy [16–19]. It is also known that 4AMP is an interesting flexible amino methyl group that can adopt four discrete conformations. The numbering of atoms in 4AMP is given in Fig. 2. The calculated structural parameters are presented in Supplementary data (S1). Since the crystal data of 4AMP is not available, the optimized geometrical parameters of the title molecule are compared with other similar systems of piperidine [20] and X-ray data of the complexes $[(H_2TMDP)_2(Bi_2I_9)]$ [21]. All the C–H bond lengths are around 1.1 Å, while the experimental value from the neutron diffraction method would be 1.098 Å [22].

Generally, the C–N–C bond angles are slightly larger than the C–C–C or N–C–C bond angles [15]. Gundersen and Rankin reported the C–N–C (110.7°), C–C–C (109.6°) and N–C–C (110.5°) bond angles by using electron diffraction technique [20]. In the present study, the bond angles of C–N–C (112.2°), C–C–C (111.5°) and N–C–C (114.2°) by B3LYP method are depicted, in Supplementary data (S1). The C–N bond lengths are predicted to be slightly shorter than the C–C bond lengths. Gundersen and Rankin [20] reported N–C (1.469 Å) and C–C (1.530 Å) by using electron diffraction technique to be approximately equal to the calculated bond length of N–C (1.466 Å and 1.465 Å) and C–C (1.54 Å and 1.539 Å) by B3LYP/6-311+G(d,p) method. We have noticed that the DFT

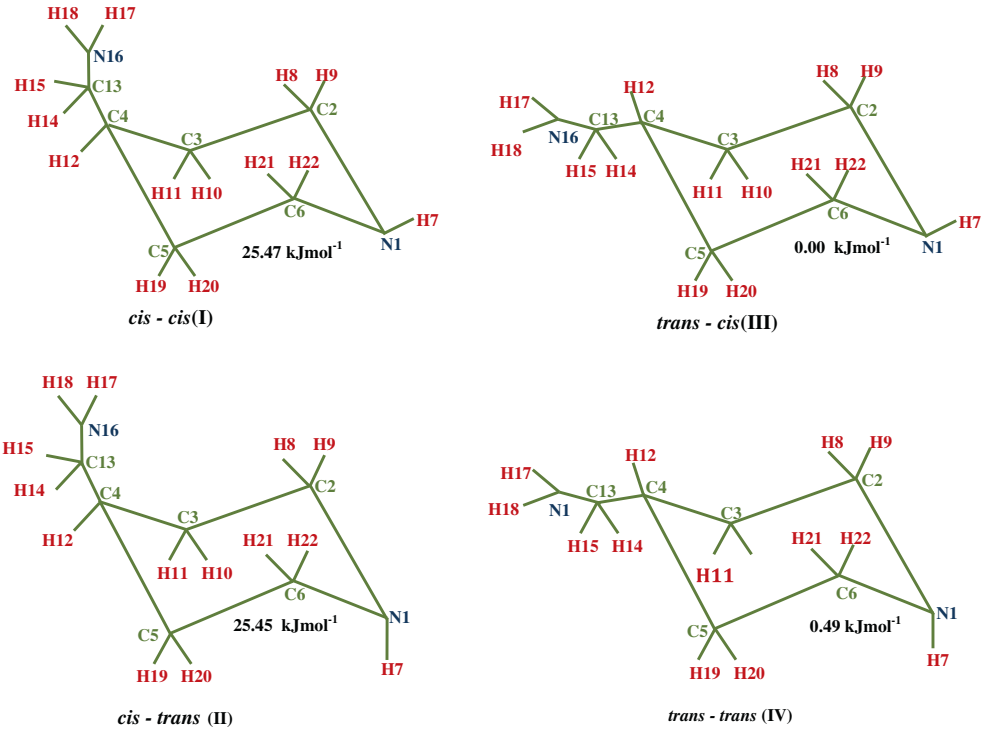

Fig. 1. Possible conformers of 4-Aminomethylpiperidine (4AMP).

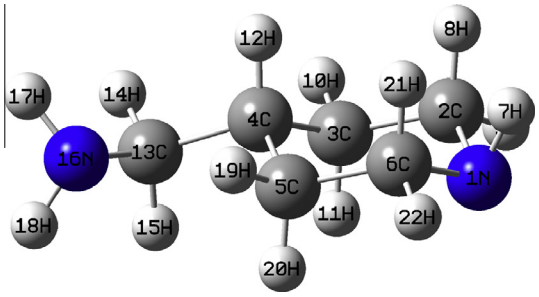

Fig. 2. The optimized structure of 4AMP.

calculations are consistent with the results of electron diffraction data [21].

In a cyclohexane ring the carbon chain is generally constrained to two conformations known as boat and chair. The pure and substituted forms of energetically favored boat or chair conformations of cyclohexane derivatives are already reported [22,23]. 4AMP consists of a six-member ring containing four methylene bridges (–CH_2–), one amine bridge (–NH–) and substituted amino methyl group at fourth position exhibits the chair conformation with computed values of dihedral angles C6–N1–C2–C3, C2–N1–C6–C5, N1–C2–C3–C4, C2–C3–C4–C5, C3–C4–C5–C6 and C4–C5–C6–N1 are 51.9°, −52.1°, −53.1°, 52.4°, −52.4° and 53.4° respectively. It can be concluded that the chair form arises due to the van der Waals repulsion between the hydrogen atoms belonging to neighboring carbon atoms. In order to reduce these interactions the hydrogen atoms in the methylene group H8–C2–H9 occupy the position farther from the hydrogen atom of the neighboring methylene groups H10–C3–H11, similarly the hydrogen atoms in the methylene group H20–C5–H19 occupy the position farther from the hydrogen atom of the neighboring methylene groups H22–C6–H21. So it loses its planarity and the calculated C–C bond lengths are almost equal. Hence the 4AMP ring chair conformation is pure chair structure as shown in Fig. 2.

PES scan studies

The 4AMP molecule can adopt different conformations, mainly by flipping the N–H bond and amino methyl substitution. Rotation at C4–C13 bond of dihedral angle C5–C4–C13–N16 leads to two conformers (I, III) at N–H bond in axial position. Similarly N–H bond in equatorial gives two conformers (II, IV). The four conformers can be assigned as *cis–cis*(I), *cis–trans*(II), *trans–cis*(III) and *trans–trans*(IV). These four conformers are influenced by different structural factors, such as steric, dipolar, inductive and hyperconjugative effects including hydrogen bonding interactions.

The potential energy scan has been performed on the optimized geometry by rotating different spatially important groups with respect to single bond present in 4AMP between 0° and 360° with the increment of 10°. The possible maxima and minima relative energies and the corresponding dihedral angles are listed in Supplementary data (S2). The PES scan plot for the type (I, II, III and IV) are given in Fig. 3. The staggered condition (60°) and the eclipsed condition (120°) correspond to the conformer (II). Comparing to the eclipsed structure the *cis–trans* staggered conformer, which corresponds to the optimized structure, is stabilized by 20.22 kJ mol^{-1}. The amine (–NH_2) nitrogen N16 which can also interact via electron, withdraws inductive effect and as a result the methyl group will have an extended conjugation with the pyridine rings. The steric strain however does not allow a planar structure which reduces the resonance stabilization via the extended conjugation and can be observed by the various dihedral angles given in the optimized structure (Supplementary data (S1)).

The energy curve for the all conformer (I, II, III and IV) and the corresponding conformers for the rotation of dihedral angle C5–C4–C13–N16 (C4–C13 bond) of 4AMP is shown in Fig. 3(a, b, c and d). It shows that the conformer from 0° to 360° rotation give many hindrances. Steric hindrance occurs when the larger size of group (–CH_3) within a molecule prevents chemical reactions that are observed in related molecules with smaller group (–NH_2). The steric interactions due to van der Waals' repulsion are

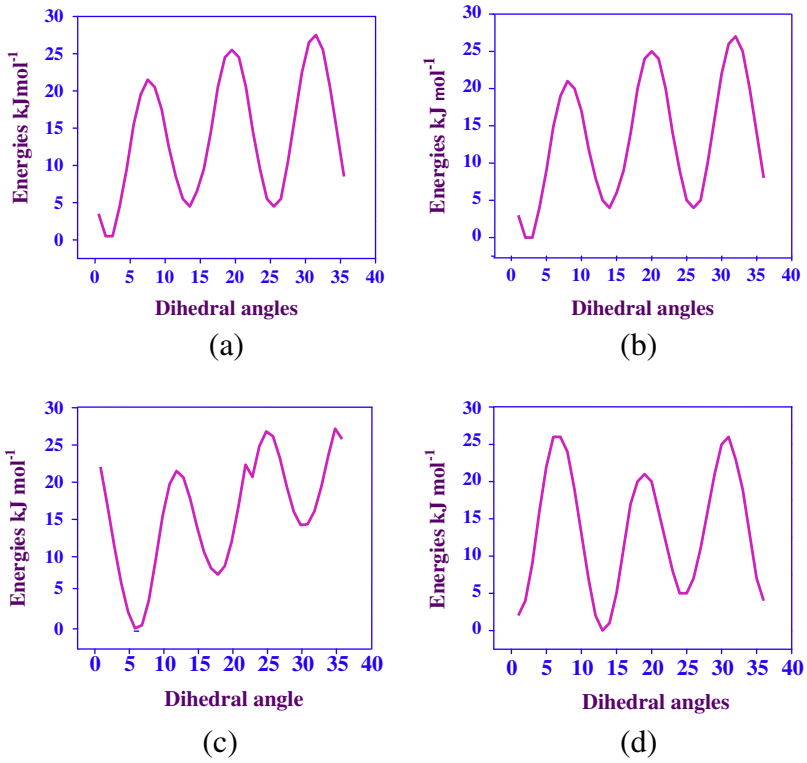

Fig. 3. PES scan for the selected degree.

comparatively weak since the distances between the interacting groups are larger.

From the II type throughout the rotation of amino methyl group, the structure remains in conformer (III). Two energy barriers of 0.25 kJ mol^{-1} and 25.88 kJ mol^{-1} (Supplementary data (S2)) are observed at 130° and 310° exactly at 180° difference, which is due to van der Waals' repulsion between nonbonded hydrogen atoms. The PES plot and the corresponding conformer for the type (a, b) is given in Fig. 3. The *cis* conformation condition (30°) and the *trans* conformation condition (220°) correspond to the *cis–cis* conformer (I).

Natural bond orbital (NBO) analysis

NBO analysis has been performed on the molecule 4AMP to identify and explain the formation of the strong intramolecular bonding between amino, amine group and carbon. The corresponding results have been tabulated in Supplementary data (S3). The importance of hyperconjugative interaction and electron density transfer (EDT) from lone electron pairs of Y atom to the X–H antibonding orbital in the X–H···Y system have been reported [24].

Supplementary data (S3) shows calculated natural orbital occupancy (number of electron (or) "natural population" of the orbital). It is noted that the maximum occupancies 1.9954, 1.9911, 1.9897, 1.9890, 1.9889, 1.9886 and 1.9884 are obtained for BD(1)C13–N16, BD(1)N16–H17, BD(1)N16–H18, BD(1)N1–C2, BD(1)N1–C6, BD(1)C2–C3 and BD(1)C5–C6, respectively, and corresponding *sp* composition are also tabulated. Therefore, the results suggest that the C13–N16, N16–H17, N16–H18, N1–C2, N1–C6, C2–C3 and C5–C6 bond lengths of these compounds are essentially controlled by the *p* character of these hybrids orbital's and also by the nature of the C13–N16, N16–H17, N16–H18, N1–C2, N1–C6, C2–C3 and C5–C6 bonds.

The NBO analysis also describes the bonding in terms of natural hybrid orbital of LP(1)N1and LP(1)N16, which occupy a higher energy orbitals (−0.4486 and −0.4682 a.u.) with considerable *p*-character (83.70% and 81.30%) and high occupation number (1.9482 a.u.) and the other BD(1)C13–N16 occupy a lower energy orbital (−0.9177 a.u.) with *p*-character (76.84%) and high occupation number (1.99541 a.u.). Thus, a very close to pure *p*-type lone pair orbital participates in the electron donation to the π^*(C–C) and π^*(C–H) orbital for nitrogen lone pair to antibonding carbon–carbon and carbon–hydrogen interactions in the compound.

Electron delocalization

Delocalization of electron density between occupied Lewis-type (bond or lone pair) NBO orbitals and formally unoccupied (antibond or Rydberg) non-Lewis NBO orbitals corresponds to a stabilizing donor–acceptor interaction. The energy of this interaction can be estimated by the second order perturbation theory [25]. Supplementary data (S4) lists the selected second order interaction energies (E2) are calculated between the donor–acceptor orbitals in I, II, III, and IV. The most important interaction energies, related to the resonance in the piperidine ring, are electron donation from the LP(1)N1 orbital to the antibonding acceptor BD*(1)C2–C3 and BD*(1)C5–C6 orbitals. This energy in I and II conformers are about 22.51, 22.72 and 22.05 kJ/mol, respectively, while in IV conformer dies out (only about 2.3 and 2.5 kJ/mol). This interaction clearly indicates the increase of p-electron delocalization through the N–H fragment of the molecule in I and II conformers and considerably reduction of electron delocalization due to the removing the co planarity of the N–H bond with the piperazine ring in I and II. Other important interactions are the electron donations from the BD(1)C6–H21, BD(1)N1–C6, BD(1)N1–C2 and the BD(1)N1–H7 to the BD*(1)N1–H7, from LP(1)N16 to the BD*(1)C2–H8 and BD*(1)-C3–H11, and from BD(1)N1–H7 to the BD*(1)C2–C3 and BD*(1)C5–C6. It is noteworthy that the electron donations from the LP (N1) orbital to the antibonding acceptor of BD*(1)C5–C6 somewhat reflect the hydrogen bond strength in these systems.

NHO directional analysis

The bending angles of different bonds expressed as the angle of deviation from the direction of the line joining the two nuclei centers of I, II, III and IV are given in Table 1. For maximum resonance interaction to occur N1 at I and IV, they should be in the same plane with piperazine ring. A little lower bending effect is also noticed at the C2–C3 bond of the piperazine and C4–C13 bond of the amino methyl group at I and IV. The bending of the bonds within the piperazine ring and amino methyl group attributes to the increase of strains at the active center of the compound.

Atomic charge

The charge distributions calculated by the Mulliken [26] and NBO methods for equilibrium geometry of 4AMP are given in Table 2. The charge distribution on the molecule has important influence on the vibrational spectra. The corresponding Mulliken's plot is shown in Fig. 4.

The total charge of the investigated complex is equal to zero. The calculated results reveal that the negative charge is delocalized between carbon, hydrogen and nitrogen atoms. In 4AMP molecule, the atoms constituting the hydrogen bonds possess the positive charges [27]. While all the carbon atoms in the molecule have negative charges which form the hydrogen bonds. Very similar values of positive charges are noticed for the four hydrogen pairs forming the CH_2 groups and one NH_2 group connected with carbon and nitrogen atoms of the piperidine ring. For the hydrogen atoms, the differences in calculated charge are relatively smaller. Very similar values of positive charges are observed for hydrogen atoms connected with carbon atoms of piperidine ring. It is worth mentioning that the biggest values of charge are notice for H7, H17 and H18 which are involved in hydrogen bonding (0.2002, 0.2218 and 0.2259 e, respectively). The charge increase at the hydrogen atoms taking part in hydrogen bonding (as supported by NBO analysis) is also a clear manifestation of hydrogen bonding. Large values of charge on N1, N16 (negative) and H7, H17, H18 (positive) are due to intramolecular charge transfer. Fig. 4 shows that the natural atomic charges are more sensitive to the changes in the molecular structure than Mullikan's net charges.

Polarizability and hyperpolarizability

Nonlinear optical (NLO) techniques are considered as among the most structure sensitive methods to study the molecular structures. Since the potential of organic materials for NLO devices have been proven, NLO properties of many of these compounds have been investigated by both experimental and theoretical methods. Quantum chemical calculations have been shown to be useful in the description of the relationship between the electronic structure of the systems and its NLO response. The computational approach allows the determination of molecular NLO properties as an inexpensive way to design molecules by analyzing their potential before synthesis and to determine high-order hyperpolarizability tensors of molecules.

The simplest polarizability (α), characterizes the ability of an electric field to distort the electronic distribution of a molecule. Higher order polarizabilities (hyperpolarizabilities β, γ, etc.) which describe the non-linear response of atoms and molecules. They are related to a wide range of phenomena from non-linear optics to intermolecular forces, such as the stability of chemical bonds, as well as, the conformation of molecules [28]. They made possible the determination of the elements of these tensors from derivatives of the dipole moment with respect to the electric field.

The first hyperpolarizability (β_0) and related properties (β, α_0 and $\Delta\alpha$) are calculated based on the finite-field approach. In the

Table 2
The charge distribution calculated by the Mulliken and natural bond orbital (NBO) methods.

Atoms	Atomic charges (Mulliken)	Natural charges (NBO)
N1	−0.209785	−0.67898
C2	−0.450322	−0.17549
C3	−0.176881	−0.39319
C4	0.187038	−0.22052
C5	−0.177028	−0.40111
C6	−0.50802	−0.17568
H7	0.200171	0.34841
H8	0.126058	0.15279
H9	0.162547	0.19305
H10	0.134097	0.19529
H11	0.142699	0.19364
H12	0.128312	0.18017
C13	−0.443468	−0.17247
H14	0.138877	0.17046
H15	0.142229	0.17636
N16	−0.458658	−0.85713
H17	0.221766	0.35054
H18	0.225926	0.35305
H19	0.187567	0.22504
H20	0.13616	0.19014
H21	0.126297	0.15212
H22	0.164417	0.19351

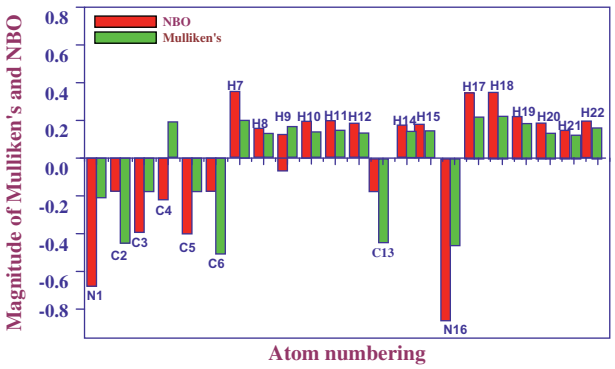

Fig. 4. Comparative graph of Mulliken's vs. natural atomic charges.

Table 1
NHO Directionality and "Bond Bending" (deviations 4AMP of nuclear centers).

NBO		Line of centers		Hybrid 1			Hybrid 2		
		θ (°)	φ (°)	θ (°)	φ (°)	Deviation at A (°)	θ (°)	φ (°)	Deviation at A (°)
BD(1)N1–C2	I	100.9	287.1	103.9	280.7	7	80.8	110.4	3.6
BD(1)N1–C6		90.8	35.3	93.1	41.9	6.9	90.4	211.9	3.6
BD(1)C2–C3	II	41.1	329.7	41.2	325.9	2.5	138.7	154.2	3
BD(1)C3–C4		85.1	35.4	82.7	33.8	2.9	91.7	217.4	3.8
BD(1)C4–C5	III	84.8	106.3	81.7	104.7	3.5	92.6	287.4	2.8
BD(1)C4–C13		144.4	349.6	142.2	347.8	2.5	34.1	170.9	1.6
BD(1)C5–C6	IV	139.7	157.5	138.5	153.5	2.8	39.4	341.1	2.5
BD(1)C13–N16		85.1	35.4	87.4	33.9	2.8	99.3	217.9	5

presence of an applied electric field, the energy of a system is a function of the electric field. The first hyperpolarizability is a third-rank tensor that can be described by a $3 \times 3 \times 3$ matrix. The 27 components of the 3D matrix can be reduced to 10 components due to the Kleinman symmetry [29]. The components of β are defined as the coefficients in the Taylor series expansion of the energy in the external electric field. When the electric field is weak and homogeneous, this expansion becomes,

$$E = E^0 - \mu_i F_i - 1/2\alpha_{ij}F_iF_j - 1/6\beta_{ijk}F_iF_jF_k - 1/24\gamma_{ijkl}F_iF_jF_kF_l + \cdots$$

where E^0 is the energy of the unperturbed molecules, F_i is the field at the origin μ_i, α_{ij}, β_{ijk} and γ_{ijkl} are the components of dipole moment, polarizability, first and second order hyperpolarizability respectively. These studies led to the fact that *ab initio* calculations of polarizabilities and hyper polarizabilities have become available through the strong theoretical basis for analyzing molecular interactions. They made possible the determination of the elements of these tensors from derivatives of the dipole moment with respect to the electric field.

The density functional theory (DFT) provides a convenient theoretical frame work for calculating global and local indices that quantitatively describe the inherent activity of chemical species. The dipole moment can be extracted from the output of any standard electronic structure program. Many experiments are done on isotropic systems (gases, neat liquids, and solutions) where the invariant vector and scalar components are measured [30]. The total static dipole moment μ, the mean polarizability α_0, the anisotropy of the polarizability $\Delta\alpha$ and the mean first hyperpolarizability β_0, using the *x*-, *y*- and *z*-components are defined as

$$\mu = \sqrt{\left(\mu_x^2 + \mu_y^2 + \mu_z^2\right)}$$

$$\alpha_o = \frac{\alpha_{xx} + \alpha_{yy} + \alpha_{zz}}{3}$$

$$\Delta\alpha = 2^{-1/2}\left[(\alpha_{xx} - \alpha_{yy})^2 + (\alpha_{yy} - \alpha_{zz})^2 + (\alpha_{zz} - \alpha_{xx})^2 + 6\alpha_{xx}^2\right]^{1/2}$$

The other components of the polarizability (α_{xy}, α_{xz}, etc.) are not needed to obtain the isotropic quantity. The first order hyperpolarizability β was also calculated using the finite field approach theory. The components of first hyperpolarizability can be calculated using the following equation

$$\beta_i = \beta_{ijk} + \frac{1}{3}\sum(\beta_{ijj} + \beta_{jij} + \beta_{jji}), \quad (i \neq j)$$

Using the *x*, *y* and *z* components, the magnitude of the first hyperpolarizability tensor can be calculated using

$$\beta_{total} = \sqrt{\left(\beta_x^2 + \beta_y^2 + \beta_z^2\right)}$$

The complete equation for calculating the magnitude of the first hyperpolarizability from Gaussian 09 output is as follows.

$$\beta_x = \beta_{xxx} + \beta_{xyy} + \beta_{xzz}$$
$$\beta_y = \beta_{yyy} + \beta_{xxy} + \beta_{yzz}$$
$$\beta_z = \beta_{zzz} + \beta_{xxz} + \beta_{yyz}$$

The equation for average second hyperpolarizability is

$$\langle\gamma\rangle = \frac{1}{5}(\gamma_{xxxx} + \gamma_{yyyy} + \gamma_{zzzz} + 2\gamma_{xxyy} + 2\gamma_{xxzz} + 2\gamma_{yyzz})$$

The theoretical second order hyperpolarizability was calculated using Gaussian 09 software. Since the value of the polarizability and hyperpolarizability of Gaussian 09 output are reported in a atomic mass units (a.u.), the calculated values have been converted into electrostatic units (esu) (α: 1 a.u. = 0.1482×10^{-24} esu; β: 1 a.u. = 8.6393×10^{-33} esu) [31]. The calculated values of β, γ and the corresponding components are given in Table 3. Urea is one of the prototypical molecules used in the study of the NLO properties of molecular systems. Therefore it was used frequently as a threshold value for comparative purposes. The first hyperpolarizability value is ca. 6.6 times smaller than urea. The β value of urea was 780.324×10^{-33} esu obtained by using B3LYP/6-311++G(d,p) method.

Molecular electrostatic potential (MEP) surface

Molecular electrostatic potentials have been used for interpreting and predicting the reactive behavior of a wide variety of chemical systems in both electrophilic and nucleophilic reactions, the study of biological recognition processes and hydrogen bonding interactions [32]. The emphasis of these studies has been on negative regions of $V(r)$. In the majority of the potential electrostatic maps the regions of negative values account for the local minima and are site candidates of electrophilic attack. The positive regions have maxima only in the nuclear positions indicating that there is no affinity by nucleophilic relatives. Fig. 6 shows the computationally observed MEP surface map with the fitting point charges to the electrostatic potential $V(r)$ for 4AMP. The electrostatic potential $V(r)$, at a given point $r(x,y,z)$ in the vicinity of a molecule, is defined in terms of the interaction energy between the electrical charge generated from the molecule electrons and nuclei and a positive test charge (a proton) located at *r*. For the systems studied the MEP values were calculated using the equation

$$V(r) = \sum \frac{Z_A}{|R_A - r|} - \int \frac{\rho(r')}{|r' - r|}dr$$

where the summation runs over all the nuclei *A* in the compound and polarization and reorganization effects is neglected. Z_A is the charge of the nucleus *A*, located at R_A and $\rho(r')$ is the electron density function of the molecule.

In the MEP surface, the region with red color is regarded as most electronegative (electrophilic) region and the region with blue color is most positive (nucleophilic) region where as the bluish green color surrounded by the ring system of 4AMP is related to less positive region.

In Fig. 5, this molecule has several possible sites for electrophilic attacks over the nitrogen atoms: N1 and N16. The average maximum negative electrostatic potential value for these electrophilic sites calculated at B3LYP/6-311+G(d,p) are about −18.43 a.u. The fitting point charges to those electrostatic potentials are −0.8564 e (N1) and −0.8964 e (N16). In the title molecule, the hydrogen atom connected to the ring system of piperidine is having less positive charge. Besides, the hydrogen atom H17 and H18 in 4AMP is surrounded by most nucleophilic region. Similarly, the fitting point charge corresponding to C4 atom is reported as high positive as

Table 3
Calculated hyperpolarizability values of 4AMP.

Parameters	Values (a.u.)	Parameters	Values (a.u.)
β_{xxx}	15.19	γ_{xxxx}	−1338.14
β_{yyy}	4.2515	γ_{yyyy}	−390.736
β_{zzz}	0.1529	γ_{zzzz}	−122.585
β_{xyy}	−2.6952	γ_{xxyy}	−225.982
β_{xxy}	2.1343	γ_{xxzz}	176.1107
β_{xxz}	0.38	γ_{yyzz}	−88.5365
β_{xzz}	−1.2231	Average γ	−425.655
β_{yzz}	1.4987		
β_{yyz}	−0.1615		
β_{xyz}	−0.4512		
β_{tot}	13.76061		

	V(r)	Point Charges (e)
N1	-18.4325	-0.8564
N16	-18.4234	-0.8964
C5	-14.8059	-0.0361
C3	-14.7944	-0.3536
C4	-14.7889	0.5194
C6	-14.7676	0.2965
C2	-14.7632	0.4977
C13	-14.7606	0.1020
H19	-1.1503	-0.0765
H20	-1.1436	0.0449
H12	-1.1389	-0.0894
H22	-1.1369	0.0005
H11	-1.1356	0.0774
H9	-1.1334	-0.0292
H10	-1.1334	-0.0080
H21	-1.1329	-0.0537
H14	-1.1309	-0.0071
H8	-1.1294	-0.1013
H15	-1.1253	0.0024
H7	-1.0707	0.2958
H17	-1.0683	0.3354
H18	-1.0682	0.3355

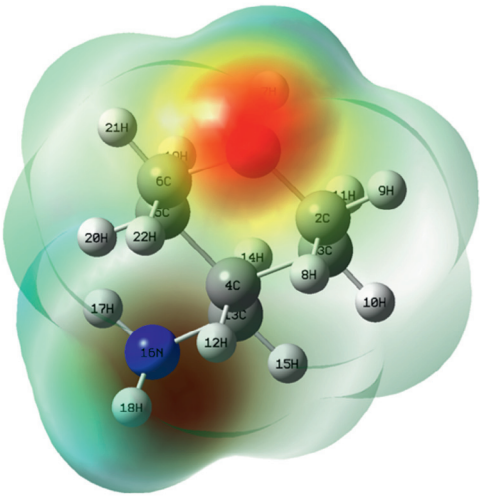

Fig. 5. Electrostatic potential surface map of 4AMP.

0.5194 e in 4AMP. N1 atom is reported as the most negative charge. Hence the atom surrounded by nitrogen atom (N1) of piperidine ring appears red color[1]. However, the nucleophilic hydrogen atoms do not appear red color. This is due to the fact that, the nucleophilic atoms are coupled together with more positive adjacent regions. Finally, we have concluded both MEP and NBO atomic charge distributions are used for predicting electrophilic and nucleophilic sites of 4AMP.

Vibrational frequencies and normal coordinate analysis

There are 60 fundamental modes of vibrations associated with 4AMP molecule. In agreement with C1 symmetry, all the 60 vibrations are distributed as 54 in-plane and 6 out-of-plane vibrations of same symmetry species. For visual representation, the observed FT-IR and FT-Raman spectra of 4AMP is shown in Figs. 6 and 7. A detailed description of the vibrational modes can be given by means of normal coordinate analysis (NCA). For this purpose, the full sets of 68 standard internal coordinates (containing 8 redundancies) are defined as given in Supplementary data (S5). From the full set 68 internal coordinates, a non-redundant set of local symmetry coordinates are constructed by means of suitable linear combinations of internal coordinates followed by the recommendation of Fogarasi and Pulay [33,34]. The local symmetry co-ordinates corresponding to probable degrees of freedom of 4AMP are presented in Supplementary data (S6). NCA is carried out for the 4AMP molecule to provide assignment of the fundamental frequencies. A computer program was written for this purpose by following Wilson's method [35]. The Cartesian coordinates for 4AMP together with the normal modes (in

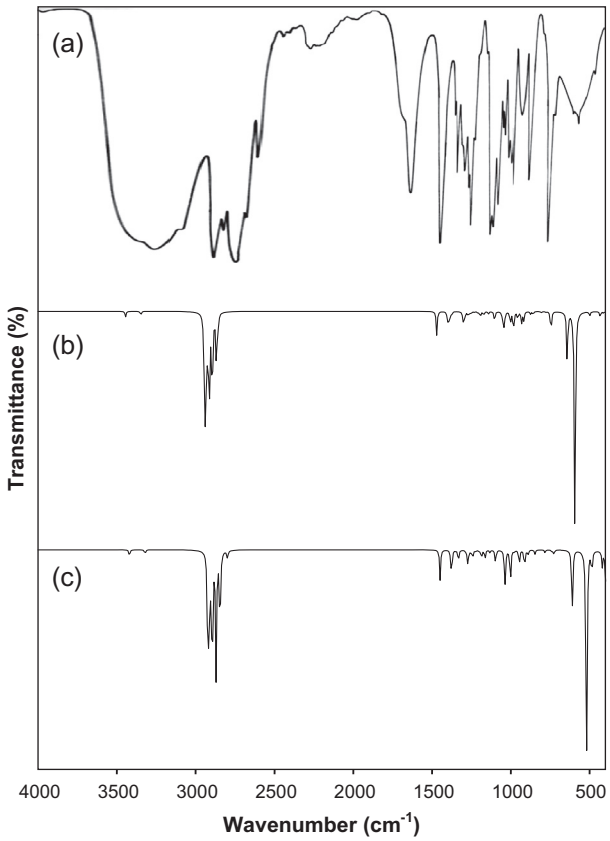

Fig. 6. Observed (a) and calculated ((b) and (c)) FT-IR spectrum of 4 AMP.

[1] For interpretation of color in Fig. 5, the reader is referred to the web version of this article.

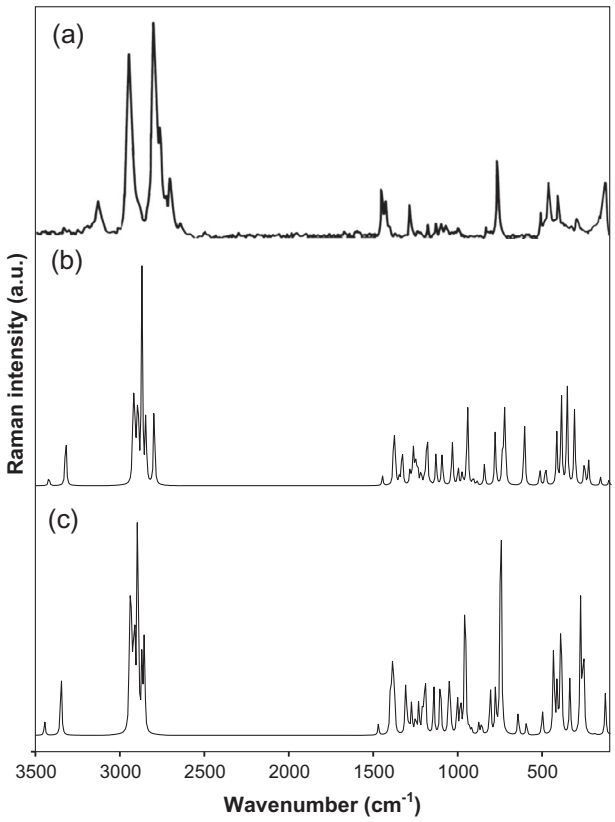

Fig. 7. Observed (a) and calculated ((b) and (c)) FT-Raman spectrum of 4 AMP.

Cartesian coordinates) and frequencies from the Gaussian 09W output were used as input in the program. The normal modes were next transformed to mass weighted Cartesian coordinates, which were then used to calculate the force constant matrix. This was diagonalized and its eigenvectors and Eigen values were used in the further calculations. Following this step the force constant matrix was transformed to internal coordinates. To ensure correctness, this transformation was checked numerically in both directions.

At this point the force constant matrix in internal coordinates could be scaled is desired, transformed back to mass-weighted Cartesians and diagonalized again to get scaled frequencies and normal modes. The matrix was finally transformed to symmetry coordinates where again all possible numerical checks were performed. In the nest step the normal modes were also transformed to symmetry coordinates. Finally, the PED for each normal mode among the symmetry coordinates is calculated and given in Table 4.

Vibrations of –NH_2 and –NH

The methyl and amino groups are generally referred as electron donating substituents in aromatic ring systems [36]. The NH_2 group gives rise to the six internal modes of vibrations as: the symmetric stretching, the antisymmetric stretching, the symmetric deformation or the scissoring, the rocking, the wagging and the torsional modes. The molecule under investigation possesses only one NH_2 group and hence expects one symmetric and one asymmetric N–H stretching vibrations in NH_2 group. The antisymmetric stretching for the CH_2, NH_2 and CH_3 has magnitude higher than the symmetric stretching [37]. The symmetric stretching, the antisymmetric stretching modes are easily assigned owing to their characteristic magnitudes in amino substituted benzenes. For saturated amines, it is established that the asymmetric NH_2 stretch will give rise to a band between 3300 and 3500 cm^{-1} [38]. The Raman spectrum shows a weak band observed at 3421 cm^{-1} corresponding to NH_2 asymmetric stretching mode. The symmetric stretching also observed as weak intense shoulder in Raman spectrum at 3328 cm^{-1}. The *ab initio* computations give the frequency of these bands at 3420 cm^{-1} for NH_2 asymmetric stretch and 3322 cm^{-1} for the symmetric stretch. The observed NH_2 stretching frequencies are higher from the computed frequencies due to the steric interactions (depends upon the substituents are in the axial or equatorial).

Heterocyclic compounds containing an N–H group exhibit N–H stretching absorption in the region from 3500 to 3200 cm^{-1} [39]. The stretching vibration of the N–H group was observed at 3325 cm^{-1}. These vibrations were calculated at 3319 cm^{-1} for B3LYP/6-311+G(d,p) method and 3347 cm^{-1} for HF/6-311+G(d,p) method. The NH_2 scissoring vibration is assigned 1446 cm^{-1} in IR spectrum. The rocking mode of the NH_2 group appears in the range 1000–1100 cm^{-1} with variable IR intensity [40]. The observed weak band at 1045 cm^{-1} in Raman spectrum and 1041 cm^{-1} in B3LYP method are attributed to the appreciable contribution from the HNH angle bending suggesting its origin due to the rocking mode. The wagging mode of the NH_2 group appears in the range 600–800 cm^{-1}. The observed weak band at 519 cm^{-1} in Raman spectrum and the band at 520 cm^{-1} in B3LYP method correspond to the NH_2 wagging mode. The observed band at 197 cm^{-1} in B3LYP method is assigned to the torsional mode of amino group vibration. The frequency observed at 489 cm^{-1} in Raman is assigned to C–NH_2 out-of-plane bending mode. The C–NH_2 in-plane vibration is assigned to 256 cm^{-1} in Raman spectrum.

C–N vibrations

The assignment of C–N stretching frequency is a rather difficult task since there are problems in identifying these frequencies from other vibrations. Silverstein et al. [41] assigned C–N stretching vibrations in the region 1382–1266 cm^{-1} for the aromatic amines. For N-methylmaleimide, Parker [40] observed the bands at 1388 and 1254 cm^{-1} in FT-IR and at 1384 and 1254 cm^{-1} in FT-Raman and assigned to C–N symmetric and asymmetric stretching vibrations, respectively. The stretching of CN modes are observed at 1180–1100 cm^{-1} region for piperidine [42,43]. We assigned this band obtained at 1103, 1041, 1003 and 1097, 1039, 1003 cm^{-1} in HF and DFT methods, respectively. The bands obtained at 1106, 1010 cm^{-1} in FT-IR spectrum and 1045 cm^{-1} in FT-Raman spectra have been assigned to CN stretching vibrations. The PED contribution results at the last column of Table 4 show, CN stretching vibrations (65%) interacting considerably with CC (37%) stretching mode.

Vibrations of cyclohexanone (CH, CH_2)

The infrared bands observed at 2980–2900 cm^{-1} region are assigned CH stretching for piperidine [42,43]. In the 1,3-bis(4-piperidyl)propane [39], the stretching of CH modes was experimentally observed at 2799–2930 cm^{-1} region. These modes were theoretically calculated at 2790–2968 cm^{-1} region for B3LYP/6-311+G(d,p) calculation [39]. In the 4AMP, the stretching of CH modes was observed at 2796 in Raman spectrum. For the assignment of CH_2 group frequencies, basically six fundamentals can be associated to each CH_2 group namely CH_2 ss, CH_2 ass, CH_2 scissoring and CH_2 rocking which belongs to in-plane vibration and two out-of-plane vibrations viz. CH_2 wagging and CH_2 twisting modes and are expected to be depolarized [44]. The asymmetric CH_2 stretching vibrations are generally observed below 3000 cm^{-1}, while the symmetric stretch will appear between 3000 and

Table 4
Vibrational assignments, infrared intensities, Raman activities and Raman intensity of 4-Aminomethylpiperidine based on HF and B3LYP/6-311+G(d,p).

Observed frequencies (cm^{-1})		Calculated frequencies (cm^{-1})				Reduced mass (amu)		Force constant (mdyneA^{-1})		IR intensity ((km) mol^{-1})		Raman activity A^0 (amu)		Raman intensity ((km) mol^{-1})		Assignments (%PED)
FTIR	FT-Raman	Unscaled		Scaled												
		a	b	a	b	a	b	a	b	a	b	a	b	a	b	
	3421	3795	3738	3445	3420	1.10	1.10	9.33	9.04	6.83	5.45	33.05	32.65	7.23	7.74	NH_{2ass}(100)
	3328	3689	3631	3349	3322	1.05	1.05	8.40	8.12	2.68	2.11	81.60	92.70	19.79	24.38	NH_{2ss}(100)
	3325	3687	3627	3347	3319	1.08	1.07	8.62	8.33	1.45	1.13	65.94	78.14	16.02	20.59	NH_{str}(99)
	2921	3242	3171	2943	2923	1.11	1.11	6.86	6.55	104.1	63.95	74.56	91.29	27.82	36.93	CH_{2ass}(98)
2919		3239	3169	2941	2921	1.11	1.11	6.84	6.54	47.71	32.26	82.67	88.43	30.93	35.87	CH_{2ass}(96)
		3232	3161	2934	2914	1.11	1.11	6.81	6.51	61.09	42.38	115.5	90.20	43.51	36.84	CH_{2ass}(97)
		3218	3145	2922	2900	1.10	1.10	6.69	6.40	70.25	56.67	111.0	114.6	42.38	47.44	CH_{2ass}(98)
		3207	3137	2912	2892	1.09	1.10	6.62	6.37	82.98	60.68	89.74	84.64	34.62	35.41	CH_{2ass}(94)
		3190	3115	2896	2871	1.07	1.06	6.40	6.08	6.74	26.52	255.0	235.2	100.0	100.0	CH_{2ss}(92)
		3189	3113	2895	2870	1.06	1.06	6.36	6.05	80.77	40.82	24.85	93.54	9.75	39.81	CH_{2ss}(91)
		3185	3112	2892	2869	1.07	1.06	6.38	6.06	21.78	37.00	38.72	38.18	15.26	16.31	CH_{2ss}(95)
2850		3161	3089	2870	2848	1.06	1.06	6.26	5.97	45.86	35.44	75.72	99.91	30.53	43.68	CH_{2ss}(92)
	2843	3154	3083	2864	2842	1.06	1.06	6.24	5.94	22.94	29.26	11.90	13.51	4.83	5.95	CH_{2ss}(92)
	2796	3145	3075	2855	2798	1.08	1.08	6.31	6.02	9.26	6.81	104.1	136.4	42.62	60.55	CH_{str}(88), CC_{str}(12)
1446		1791	1630	1470	1449	1.10	1.10	2.09	1.71	28.04	24.37	2.16	2.73	3.40	4.66	NH_{2sciss}
1387		1620	1478	1401	1384	1.21	1.10	1.87	1.41	10.96	1.07	0.59	7.31	1.12	15.09	CCH_{bend}(72)
	1371	1617	1473	1399	1379	1.10	1.09	1.69	1.39	0.18	10.35	5.36	3.75	10.24	7.77	CH_{2sciss}(87)
1364		1609	1470	1392	1376	1.09	1.12	1.67	1.43	8.67	3.29	3.99	7.39	7.69	15.44	CH_{2sciss}(88)
		1604	1467	1387	1373	1.10	1.09	1.66	1.39	3.04	5.58	2.89	1.20	5.60	2.52	CH_{2sciss}(80)
	1359	1603	1465	1386	1350	1.09	1.09	1.65	1.38	1.42	0.38	6.14	1.69	11.92	3.56	CH_{2sciss}(88)
1340		1591	1447	1376	1333	1.10	1.14	1.64	1.40	3.85	9.78	10.38	10.61	20.42	22.63	CH_{2sciss}(78)
1290		1514	1373	1309	1286	1.57	1.39	2.13	1.54	1.97	0.97	6.29	3.51	13.53	8.18	CH_{2wagg}(35)
	1281	1507	1362	1303	1278	1.42	1.41	1.90	1.54	0.17	8.42	1.64	0.91	3.56	2.14	CH_{2wagg}(31)
		1502	1358	1299	1274	1.42	1.23	1.89	1.34	18.27	3.89	1.80	0.74	3.93	1.75	CH_{2wagg}(46)
		1489	1351	1288	1269	1.24	1.41	1.62	1.51	2.31	1.86	0.74	8.34	1.64	20.03	CH_{2wagg}(16)
1263		1473	1336	1274	1262	1.29	1.29	1.65	1.36	2.73	1.44	4.11	3.87	9.28	9.47	CH_{2wagg}(48)
		1462	1328	1264	1244	1.29	1.23	1.62	1.28	3.67	2.31	0.46	1.73	1.05	4.29	CCH_{bend}(48)
		1445	1324	1250	1240	1.23	1.29	1.51	1.33	2.26	3.76	2.58	2.05	6.02	5.19	CH_{2twist}(44)
1230		1423	1300	1231	1222	1.33	1.37	1.59	1.36	0.95	1.15	4.13	2.87	9.90	7.46	CH_{2twist}(43)
	1212	1397	1277	1208	1206	1.28	1.33	1.48	1.27	1.82	1.17	4.45	1.89	11.01	5.07	CH_{2twist}(35)
1195		1379	1262	1193	1196	1.25	1.29	1.41	1.21	6.72	6.97	9.15	11.23	23.14	30.79	CH_{2twist}(45)
1169		1337	1224	1172	1164	1.27	1.36	1.34	1.20	4.66	7.44	0.17	0.23	0.45	0.66	CH_{2twist}(62)
1143		1302	1191	1142	1138	1.87	2.07	1.87	1.73	2.80	2.17	5.32	4.97	14.81	15.00	CH_{2twist}(54)
1106		1244	1153	1103	1097	1.77	2.36	1.61	1.85	12.59	10.85	6.89	5.22	20.67	16.98	CN_{str}(62), R_{bend}(51)
		1188	1092	1054	1049	1.53	2.83	1.27	1.99	5.12	10.71	3.61	2.77	11.66	9.70	CC_{str}(40)
	1047	1182	1091	1048	1042	1.72	2.24	1.41	1.57	9.18	15.51	3.45	2.28	11.24	8.05	CC_{str}(48)
	1045	1174	1089	1041	1039	3.15	1.41	2.56	0.99	18.07	5.74	1.14	1.52	3.75	5.43	CN_{str}(55) + HNH_{bend}(20)
1010		1131	1054	1003	1003	1.56	3.24	1.18	2.12	13.65	26.12	3.48	2.36	12.16	8.94	CN_{str}(65) + CC_{str}(37)
985		1108	1028	983	978	3.09	1.40	2.24	0.87	25.10	1.27	3.23	1.65	11.65	6.45	CN_{str}(97)
953		1066	996	956	947	1.98	2.21	1.32	1.29	8.98	11.47	13.86	10.34	53.08	42.94	CC_{str}(79)
		1039	960	932	913	1.83	2.43	1.16	1.32	14.05	14.19	0.36	0.86	1.43	3.71	CC_{str}(74)
894		1023	937	918	891	1.94	1.82	1.20	0.94	11.18	4.01	0.38	0.45	1.55	1.99	CH_{2rock}(72)
		976	891	875	848	1.50	1.84	0.84	0.86	3.04	1.73	0.73	1.01	3.20	4.80	CH_{2rock}(81), CC(23)
848		957	889	858	846	2.17	1.68	1.17	0.78	3.32	1.94	0.81	0.96	3.65	4.70	CH_{2rock}(85)
782		900	823	807	783	1.78	1.80	0.85	0.72	1.57	2.36	3.02	4.45	14.93	23.85	δRing(67)
		865	777	776	739	1.58	1.77	0.70	0.63	0.72	1.72	2.38	3.50	12.48	19.89	CH_{2rock}(83)
		831	763	745	726	2.61	2.03	1.06	0.70	24.69	3.55	14.93	6.33	83.01	38.16	δRing(51)
598	602	802	642	642	611	1.52	1.92	0.58	0.47	67.70	55.57	1.18	4.79	6.91	30.41	NH_{2sciss}(85)
	519	740	559	593	520	1.41	1.77	0.45	0.33	312.9	200.3	0.56	1.01	3.68	7.21	NH_{2wagg}(78)
	489	623	527	499	486	1.63	1.95	0.37	0.32	5.42	17.07	0.87	1.00	7.34	9.14	CH_{2rock}(82)
	437	518	456	432	420	2.86	2.42	0.45	0.30	6.14	12.42	2.37	1.71	26.10	20.42	Ring breathing(21)
		494	427	412	393	2.73	1.54	0.39	0.17	1.75	77.97	1.09	2.85	12.87	36.47	δRing(48)
	359	466	397	389	358	1.75	1.89	0.22	0.18	4.55	42.40	3.02	2.89	38.84	40.29	γ CCH(59), CNC $_{bend}$(27)
	321	402	349	336	314	1.17	2.96	0.11	0.21	40.99	16.79	0.86	1.77	13.78	30.75	CNC(6), CCC(6) bend
	256	382	284	272	256	2.85	1.56	0.25	0.07	6.28	13.04	2.03	0.60	35.13	11.26	CNH_{2rock}(78)
		358	203	255	231	1.85	2.45	0.14	0.06	1.17	1.69	1.42	0.45	27.13	9.32	γ Ring(32)
	161	263	185	187	161	1.73	1.69	0.07	0.03	0.06	0.70	0.01	0.09	0.31	3.03	γ Ring(37)
	111	247	123	116	111	2.62	2.10	0.09	0.02	1.15	5.97	0.29	0.05	9.96	1.86	CNC_{bend}(17), CCC_{bend}(13)
		197	57	61	52	2.38	2.75	0.05	0.01	1.50	3.74	0.05	0.04	2.50	2.17	NH_{2twist}(75)
		145	48	54	41	3.10	1.04	0.04	0.03	1.71	37.58	0.02	0.35	1.69	32.10	γ Ring (35) + γ CCC(30)

Intensities: w – weak, vw – very weak, s – strong, vs – very strong, str – stretching, ss – symmetric stretching, ass – asymmetric stretching, δ – in-plane bending, γ – out-of-plane bending, sciss. – scissoring, wag. – wagging, rock. – rocking, bend – bending. a: Calculated by HF/6-311+G(d,p) and b: Calculated by B3LYP/6-311+G(d,p).

2700 cm^{-1} [45–47]. The CH_2 asymmetric stretching vibrations are observed at 2943, 2941, 2934, 2922, 2912 and 2923, 2921, 2914, 2900, 2892 cm^{-1} in HF and DFT methods, respectively. They are very pure modes since their PED contributions are above 92%. The scissoring vibrations involving C2, C3, C5, C6 and C13 can be observed in IR band at 1364, 1340 cm^{-1} and Raman band at

1359 cm^{-1} respectively. The CH_2 scissoring modes were observed at 1399, 1392, 1387, 1386, 1376 and 1379, 1376, 1373, 1350, 1333 cm^{-1} in DFT and HF method, respectively. The band at 894, 848, 598 cm^{-1} in FT-IR and 602 cm^{-1} in FT-Raman is assigned to CH_2 rocking vibration. The CH_2 twisting bending vibrations are observed at 1230, 1195, 1169, 1143 cm^{-1} in FT-IR and 1212 cm^{-1} in FT-Raman. The bands observed at 1290, 1263 cm^{-1} in FT-IR and 1281 cm^{-1} in FT-Raman spectra are assigned to CH_2 wagging vibration.

Ring vibrations

Piperidine ring CC stretching modes were shown at 1350–760 cm^{-1} region [42,43]. In the 1,3-bis(4-piperidyl) propane, the stretching vibrations of the CC was calculated at 1067–1088 cm^{-1} region for B3LYP/6-311+G(d,p) [39]. In case of 4AMP, the carbon atoms coupled together in the hexagonal chain of ring possesses four C–C stretching vibrations at 953 and 1047 cm^{-1} in FT-IR and FT-Raman. The in-plane and out-of-plane bending vibrations of the benzene ring are generally observed below 1000 cm^{-1} [48] and these modes are not pure but they contributes drastically from other vibrations and are substituent-sensitive. In the title molecule, the ring in-plane (δ_{ring}) and out-of plane (γ_{ring}) bending modes are affected to a great extent by the substituents and produce bands below 600 cm^{-1}. From PED results, the bands present at 437, 161 and 782 cm^{-1} in FT-Raman and FT-IR spectra are assigned to γ_{ring}. The scaled theoretical wavenumbers corresponding to all the ring vibrations are found to have a good correlation with their available experimental observations.

Theoretical UV–Visible spectra and solvent effect

In order to investigate the electron transition between the energy levels, the lowest singlet → singlet spin allowed excited states are to be taken into account. In the present study, the maximum absorption wavelengths (λ_{max}), excitation energies (ΔE) and oscillator strengths (f) of the title molecules in the gas and solvent (DMSO and Acetone) phase are computed using TD-DFT/B3LYP/6-311+G(d,p). The observed peaks in the spectrum may cause one electron excitation from HOMO → LUMO, HOMO−1 → LUMO and HOMO−2 → LUMO.

The solvent effect on the absorption wavelengths and excitation energies are also examined by applying polarizable continuum model (PCM) TD-DFT method with B3LYP/6-311+G(d,p) basis set. The calculated absorption wavelengths, oscillator strengths, excitation energies of molecule in gas, DMSO and methanol solvent medium are presented in Table 5 and theoretical UV–Visible spectrum of 4AMP in different solvents as shown in Fig. 8. In the electronic spectrum of 4AMP, the strong intensity peaks at the maximum absorption wavelength of 218.67 (gas), 172.76 (DMSO) and 185.86 (acetone) are caused by $\pi \rightarrow \pi^*$ transitions and the smaller intensity bands calculated above 260 nm in all the phases of 4AMP are strongly forbidden and therefore, the value of its oscillator strength nearly equals to zero.

The conjugated molecules are characterized by a small amount of highest occupied molecular orbital-lowest unoccupied molecular orbital (HOMO–LUMO) separation, which is the result of a significant degree of ICT from the end-capping electron-donor groups to the efficient electron-acceptor groups through π-conjugated path [49]. The HOMO–LUMO energy gap for 4AMP was computed at the B3LYP/6-311+G(d,p) level. The Eigen values of LUMO and HOMO and their energy gap reflect the chemical activity of the molecule. Generally, if the energy gap between the HOMO and LUMO decreases, it is easier for the electrons of the HOMO to be excited. The energy of HOMO, to easier it is for LUMO to accept electrons when the energy of LUMO is low. The total energy, energy gap and dipole moment have an effect on the stability of a molecule. We have done optimization in order to investigate the energetic behavior and dipole moment of title compound in gas phase and solvent. The total energy, dipole moment and frontier molecular orbital energies have been calculated with B3LYP/6-311+G(d,p) level. Result obtained from solvent and gas phase are listed in Supplementary data (S7). The energy values of HOMO are computed −6.54597, −10.3292, −10.3286 eV and LUMO are 0.1203, 1.9331, 1.9358 eV and energy gap values are 6.4257, 8.3955 and 8.3934 eV in gas, acetone and DMSO for 4AMP molecule, respectively. Dipole moment shows the molecular charge distribution and is given as a vector in three dimensions. Therefore, it can be used as a descriptor to depict the charge movement across the molecule. Direction of the dipole moment vector in a molecule depends on the centers of positive and negative charges. Dipole moments are strictly determined for neutral molecules. We can say that in going from the gas phase to the solvent phase, the dipole moment value increases (Supplementary data (S7)).

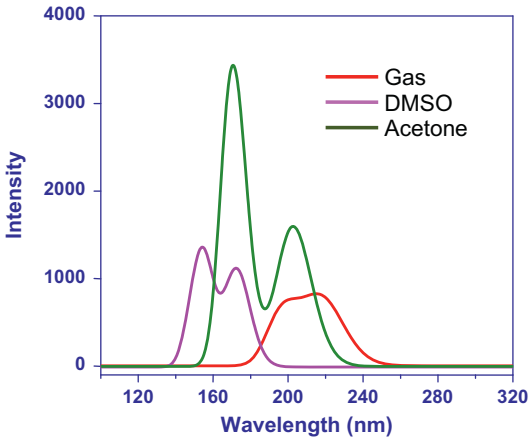

Fig. 8. Calculated UV–Visible spectra of 4AMP.

Pauling introduced the concept of electronegativity as the power of an atom in a compound to attract electrons to it. Hardness (η), chemical potential (μ), electronegativity (χ), global softness (σ), ionization potential (I), electron affinity (A) and global electrophilicity (ω) are defined as follows:

$$\eta = \frac{1}{2}\left(\frac{\partial^2 E}{\partial N^2}\right)_{V(r)} = \frac{1}{2}\left(\frac{\partial \mu}{\partial N}\right)_{V(r)}$$

Table 5
Calculated maximum absorption wavelengths (max), excitation energies (ΔE) and oscillator strengths (f) of 4AMP in gas phase and in different solvent (water and methanol) by TD-DFT/B3LYP/6-311++G(d,p) method.

Excitation level	Gas phase				Methanol		DMSO		
	max (nm)	max (nm)	ΔE (eV)	f	ΔE (eV)	f	max (nm)	ΔE (eV)	f
H–L	218.67	185.86	6.6709	0.0475	5.6698	0.0183	172.76	7.1767	0.0277
H1–L	200.26	159.63	7.7669	0.0274	6.1911	0.0036	155.48	7.9743	0.0287
H2–L	196.85	156.55	7.9199	0.0513	6.2984	0.0129	148.46	8.3516	0.0112

$$\mu = \left(\frac{\partial E}{\partial N}\right)_{V(r)}$$

$$\chi = -\mu = -\left(\frac{\partial E}{\partial N}\right)_{V(r)}$$

where E is the total energy, N is the number of electrons of the chemical species and η is the chemical potential and $V(r)$ is the external potential, which is identified as the negative of the electronegativity (χ) as defined by Iczkowski and Margrave [50]. According to Koopman's theorem [51], the entries of the HOMO and the LUMO orbital's of the molecule are related to the ionization potential (I) and the electron affinity (A), respectively, by the following relations:

$$I = -E_{\mathrm{HOMO}}$$

$$A = -E_{\mathrm{LUMO}}$$

where I and A are ionization potential and electron affinity of the compound respectively. Electron affinity refers to the capability of ligand to accept precisely one electron from a donor. However, in many kinds of bonding viz covalent hydrogen bonding, partial charge transfer takes place). Absolute electronegativity (χ) and hardness (η) of the molecule are given by [52], respectively. Softness (σ) is a property of compound that measures the extent of chemical reactivity. It is the reciprocal of hardness.

$$\chi = (\mathrm{I} + A)/2$$
$$\eta = (\mathrm{I} - A)/2$$
$$\sigma = \frac{1}{\eta}$$

Parr et al. [53] have defined global electrophilic power of the compound as electrophilicity index (ω) in terms of chemical potential and hardness as follows.

$$\omega = \left(\frac{\mu^2}{2\eta}\right)$$

All the calculated values of quantum chemical parameters of 4AMP molecules in gas and solvent phase at TD-DFT/B3LYP method with 6-311+G(d,p) basis set are presented in supplementary data (S7).

Conclusion

The present work for the proper vibrational frequency assignments for the compound of 4AMP from the FT-IR and FT-Raman spectra have been recorded for the first time. The equilibrium geometries, harmonic vibrational frequencies, IR intensities and Raman intensities of the title compound were determined and analyzed by both at HF and B3LYP levels of theory utilizing 6-311+G(d,p) basis set. Although B3LYP has performed better than HF, as far as the bond lengths are concerned, both the methods have performed nearly to the same level across the bond angle sets. We have carried out density functional theory calculations on the structure, vibrational spectra, electric dipole moment, polarizability and the hyperpolarizability, NBO, HOMO–LUMO analyses of the compound. On the basis of agreement between the calculated and experimental results assignments of all the fundamental vibrational modes of 4AMP are examined and proposed in this investigation. The electric dipole moments and first hyperpolarizability of the compound studied have been calculated by DFT method with 6-311+G(d,p) basis set. The lowering of HOMO–LUMO energy gap explains the eventual charge transfer interactions takes place within the molecule. The NBO analysis performed in this study enabled us to know about the conjugative interactions and other type of interactions taking place within the molecular species. The vibrational frequencies were calculated and scaled values have been compared with the experimental FT-IR and FT-Raman spectra.

Appendix A. Supplementary material

Supplementary data associated with this article can be found, in the online version, at http://dx.doi.org/10.1016/j.saa.2014.04.154.

References

[1] Spaeth and Englaender, Ber. 68 (1935) 2218; cf. Pictet and Pictet, Helv. Chim. Acta, 10 (1927) 593.
[2] S. Rimington, Afr. J. Sci. 31 (1934) 184–193.
[3] Juraschewski, Stepanov, J. Gen. Chem., U.R.S.S. 9 (1939) 1687.
[4] J.L. Arbiser, T. Kau, M. Konar, et al., Solenopsin, the alkaloidal component of the fire ant (*Solenopsis invicta*), is a naturally occurring inhibitor of phosphatidylinositol-3-kinase signaling and angiogenesis, Blood 109 (2007) 560–565.
[5] T.A. Henry, The Plant Alkaloids, fourth ed., The Blakiston Company, 1949.
[6] V.V. Kane, M. Jones, Org. Syn. 7 (1990) 473–476.
[7] M.B. Smith, J.M. Wiley, in: D.H. Solomon (Ed.), March's Advanced Organic Chemistry: Reactions, Mechanisms, and Structure, fifth ed., John Wiley & Sons, New York, 1968.
[8] G.P. Claxton, L. Allen, J.M. Grisar, Coll. 6 (1988) 968.
[9] C.S. Marvel, W.A. Lazier, Benzoyl piperidine, Org. Synth. Coll. 1 (1941) 99–101.
[10] B.A. Hess Jr., J. Schaad, P. Carky, R. Zaharaduick, Chem. Rev. 86 (1986) 709–730.
[11] M.J. Frisch, G.W. Trucks, H.B. Schlegel, G.E. Scuseria, M.A. Robb, J.R. Cheeseman, G. Scalmani, V. Barone, B. Mennucci, G.A. Petersson, H. Nakatsuji, M. Caricato, X. Li, H.P. Hratchian, A.F. Izmaylov, J. Bloino, G. Zheng, J.L. Sonnenberg, M. Hada, M. Ehara, K. Toyota, R. Fukuda, J. Hasegawa, M. Ishida, T. Nakajima, Y. Honda, O. Kitao, H. Nakai, T. Vreven, J.A. Montgomery Jr., J.E. Peralta, F. Ogliaro, M. Bearpark, J.J. Heyd, E. Brothers, K.N. Kudin, V.N. Staroverov, R. Kobayashi, J. Normand, K. Raghavachari, A. Rendell, J.C. Burant, S.S. Iyengar, J. Tomasi, M. Cossi, N. Rega, J.M. Millam, M. Klene, J.E. Knox, J.B. Cross, V. Bakken, C. Adamo, J. Jaramillo, R. Gomperts, R.E. Stratmann, O. Yazyev, A.J. Austin, R. Cammi, C. Pomelli, J.W. Ochterski, R.L. Martin, K. Morokuma, V.G. Zakrzewski, G.A. Voth, P. Salvador, J.J. Dannenberg, S. Dapprich, A.D. Daniels, O. Farkas, J.B. Foresman, J.V. Ortiz, J. Cioslowski, D.J. Fox, Gaussian, Inc., Wallingford CT, 2009.
[12] (a) T. Sundius, J. Vib. Spectrosc. 29 (2002) 89–95;
(b) MOLVIB: A Program for Harmonic Force Field Calculations, QCPE Program No., 2002, 807.
[13] E.D. Glendening, A.E. Reed, J.E. Carpenter, F. Weinhold, NBO Version 3.1, TCI, University of Wisconsin, Madison, 1998.
[14] J. Chocholoussova, V.V. Spirko, P. Hobza, J. Phys. Chem. 6 (2004) 37–41.
[15] E. Vayner, D.W. Ball, J. Mol. Struct. (Theochem) 496 (2000) 175–183.
[16] Yu.A. Pentin, O.S. Anisimova, Opt. Spectrosc. 26 (1968) 35.
[17] T. Hirakowa, T. Kimura, K. Ohno, H. Murata, Spectrochim. Acta A 36 (1980) 329–332.
[18] G. Marcotrigiano, L. Menabue, G.C. Pellacani, J. Mol. Struct. 30 (1976) 85.
[19] Y. Okishi, Y. Imai, K. Aida, J. Inorg. Nucl. Chem. 13 (1973) 101.
[20] G. Gundersen, D.W. Rankin, Acta Chem. Scand. A 37 (1983) 865–874.
[21] A.M. Goforth, L. Peterson, M.D. Simith, H.-C. Loye, J. Solid State Chem. 178 (2005) 3529–3540.
[22] A.E. Reed, L.A. Curtiss, F. Weinhold, Chem. Rev. 88 (1988) 899–926.
[23] J.C. Tai, N.L. Allinger, J. Am. Chem. Soc. 88 (1966) 2179.
[24] A.E. Reed, F. Weinhold, J. Chem. Phys. 83 (1985) 1736–1740.
[25] S.F. Tayyari, Z. Moosavi-Tekyeh, M. Soltanpour, A.R. Berenji, R.E. Sammelson, J. Mol. Struct. 892 (2008) 32–38.
[26] R.S. Mulliken, J. Chem. Phys. 23 (1955) 1833–1840.
[27] J.S. Murray, K. Sen, Molecular Electrostatic Potentials, Concepts and Applications, Elsevier, Amsterdam, 1996.
[28] D.M. Burland, R.D. Miller, C.A. Walsh, Chem. Rev. 94 (1994) 31–74.
[29] D.A. Kleinmen, Phys. Rev. 126 (1962) 1977–1979.
[30] B. Edwin, M. Amalanathan, I. Hubert Joe, Spectrochim. Acta A 96 (2012) 10–17.
[31] G. Mahalakshmi, V. Balachandran, J. Mol. Struct. 1063 (2014) 109–122.
[32] A. Nataraj, V. Balachandran, T. Karthick, M. Karabacak, A. Atac, J. Mol. Struct. 1027 (2012) 1–14.
[33] G. Fogarasi, X. Zhou, P.W. Taylor, P. Pulay, J. Am. Chem. Soc. 114 (1992) 8191–8201.
[34] G. Fogarasi, P. Pulay, J.R. Durig (Eds.), Vib. Spectra and Struct, vol. 14, Elsevier, Amsterdam, 1985. pp. 125–129.
[35] E.B. Wilson, J.C. Decius, P.C. Cross, Molecular Vibrations, McGraw-Hill, New York, 1995.
[36] N.B. Colthup, L.H. Daly, S.E. Wiberley, Introduction to Infrared and Raman Spectroscopy, Academic Press, New York, 1990.
[37] A.D. Becke, J. Chem. Phys. 98 (1993) 5648–5652.
[38] L.J. Bellamy, The Infrared Spectra of Complex Molecules, vol. 2, Chapman and Hall, London, 1980.
[39] Y. Erdogdu, M.T. Gulluoglu, S. Yurdakul, J. Mol. Struct. 889 (2008) 361–370.
[40] S.F. Parker, Spectrochim. Acta A 51 (1995) 2067–2072.
[41] M. Silverstein, G. Clayton Basseler, C. Morill, Spectrometric Identification of Organic Compounds, Wiley, New York, 1981.
[42] M.T. Gulluoglu, Y. Erdogdu, S. Yurdakul, J. Mol. Struct. 834 (2007) 540–547.

[43] E. Gornicka, J.E. Rode, E.D. Raczynska, B. Dasiewicz, J.C. Dobrowolski, Vib. Spectrosc. 36 (2004) 105–115.
[44] G. Varsanyi, Vibrational Spectra of Benzene Derivatives, Academic Press, New York, 1969.
[45] G. Litivinov, Proceedings of the XIII International Conference on Raman Spectroscopy, Wurzburg, Germany, 1992.
[46] K. Furie, V. Mohacek, M. Bonifacic, I. Stefanic, J. Mol. Struct. 267 (1992) 39–44.
[47] V. Balachandran, G. Mahalakshmi, A. Lakshmi, A. Janaki, Spectrochim. Acta 97 (2012) 1101–1110.
[48] S. Gunasekaran, R.A. Balaji, S. Kumaresan, G. Anand, S. Srinivasan, Can. J. Anal. Sci. Spectrosc. 53 (2008) 149–162.
[49] D. Sajan, Y. Erdogdu, Thomas Kuruvilla, I. Hubert Joe, J. Mol. Struct. 983 (2010) 1221.
[50] R.P. Iczkowski, J.V. Margrave, J. Am. Chem. Soc. 83 (1961) 3547–3551.
[51] L. Larabi, Y. Harek, O. Benali, S. Ghalam, Prog. Org. Coat. 54 (2005) 256–262.
[52] I. Lukovits, I. Bako, A. Shaban, E. Kalman, Electrochim. Acta 43 (1998) 131–136.
[53] R.G. Parr, L.V. Szentpaly, S.J. Liu, Am. Chem. Soc. 121 (1999) 1922–1924.